NANOSYSTEMS: PHYSICS, CHEMISTRY, MATHEMATICS, 2019, 10 (1), P. 70–75

Very wide-bandgap nanostructured metal oxide materials for perovskite solar cells

L. L. Larina[1], O. V. Alexeeva[1], O. V. Almjasheva[2], V. V. Gusarov[3], S. S. Kozlov[1],
A. B. Nikolskaia[1], M. F. Vildanova[1], O. I. Shevaleevskiy[1]

[1]Department of Solar Photovoltaics, Institute of Biochemical Physics RAS,
Kosygin St. 4, Moscow, 119334, Russia
[2]St. Petersburg Electrotechnical University "LETI", Professora Popova St. 5, Saint Petersburg, 197376, Russia
[3]Ioffe Physical-Technical Institute RAS, Politekhnicheskaya St. 26, Saint Petersburg, 194021, Russia
shevale2006@yahoo.com, almjasheva@mail.ru, victor.v.gusarov@gmail.com

PACS 73.63.Bd **DOI 10.17586/2220-8054-2019-10-1-70-75**

Very wide-bandgap undoped and Y_2O_3-doped ZrO_2 nanoparticles were synthesized and their structural, optical, morphological and energy characteristics were investigated. It was found that the bandgap value in ZrO_2 decreases with Y_2O_3 doping. The developed materials were used for fabrication of nanostructured photoelectrodes for perovskite solar cells (PSCs) with the architecture of glass/FTO/ZrO_2–Y_2O_3/$CH_3NH_3PbI_3$/spiro-MeOTAD/Au. The power conversion efficiency in the PSCs based on ZrO_2–Y_2O_3 photoelectrodes was significantly higher than that for undoped ZrO_2 photoelectrodes. We have found that nanostructured layers, based on very wide-bandgap materials could efficiently transfer the injected electrons via a hopping transport mechanism.

Keywords: nanostructures, ZrO_2, thin films, semiconductors, solar photovoltaics, perovskite solar cells.

Received: 10 November 2018

Revised: 18 January 2019

1. Introduction

Nanostructured materials are widely used for the development of next-generation solar cells (SCs) since they enable fabrication of high efficiency and low-cost devices which are promising for mass production of photovoltaic technologies [1, 2]. Recently, a considerable interest is focused on inorganic–organic metal halide perovskite solar cells (PSCs) in which the record power conversion efficiency (PCE) exceeded 22 % [3] and reached 27.3 % in perovskite-silicon tandem solar cell [4]. PSC's architecture comprises a mesoscopic layer of metal-oxide nanoparticles on a conductive substrate, which plays a role of the electron-conductive photoelectrode, a perovskite ($CH_3NH_3PbI_3$) layer deposited on top of the photoelectode, a hole-conductive layer and a metallic counter electrode [5, 6].

One of the key components of the PSC is an electron-conductive photoelectrode, which consists of metal oxide semiconductor nanoparticles organized in a mesoscopic architecture. Nanostructured layers of titanium dioxide (TiO_2) with the band gap (E_g) of 3.0 – 3.2 eV are generally used as photoelectrodes in PSCs [7, 8]. At the same time, some other wide-bandgap materials were also successfully used in photoelectrodes [9]. The application of a very wide-bandgap metal oxide, such as ZrO_2 with $E_g \sim 5.7$ eV, is of special interest for this purpose [10]. Condensed layers of wide-bandgap materials are dielectrics with insulator type conductivity behavior and can't be used as a conductive medium. However, their analogs with nanostructured morphology demonstrate high electron-conductive abilities, due to the large concentration of the nanoparticle surface defects. A number of publications confirmed that in nanostructured systems with $E_g > 5$ eV, the effective transfer of the injected electrons was observed, while the density of the electrons in the conduction band was negligible [9]. Charge transport through the nanostructured layer can be realized on the basis of a hopping conduction mechanism through localized states within forbidden zone [10].

The formation of crystal phase and morphology in ZrO_2 as well as optical and electrical properties of ZrO_2 nanoparticles strongly depend on the synthesis conditions [11]. A significant advantage of ZrO_2 material is its ability to be doped with yttrium oxide (Y_2O_3), which allows one to vary the optoelectronic characteristics of ZrO_2–Y_2O_3-based nanostructured systems. Doping with rare-earth metals or niobium (Nb) allows to significantly improve the transport characteristics of the photoelectode and to increase the PCE of the PSCs [12, 13]. Previously reports of PSCs fabricated using undoped ZrO_2-based photoelectode have been made [14]. In this work, we have synthesized ZrO_2 nanoparticles and yttrium oxide doped ZrO_2–Y_2O_3 systems which were used for fabrication of the nanostructured electron-conductive photoelectrodes for PSCs. Using the developed ZrO_2–Y_2O_3-based photoelectrodes, we have prepared a series of PSCs and provided comparative measurements of the main photovoltaic parameters.

2. Experimental

2.1. Materials and samples preparation

Nanocrystalline zirconium dioxide was prepared by hydrothermal treatment of zirconium oxyhydroxide precipitated from a solution of $ZrOCl_2$ (chemical pure grade) with concentrated aqueous NH_4OH. Hydrothermal treatment was performed at $T = 250$ °C and $P = 70$ MPa over 4 h. The Y_2O_3-doped ZrO_2 nanoparticles were obtained by hydrothermal treatment of co-precipitated zirconium and yttrium hydroxides from solutions of the corresponding metal salts. The conditions of hydrothermal treatment were chosen according to the data in [11] and corresponded to complete dehydration of zirconium hydroxide.

To fabricate a nanostructured photoelectrode based on ZrO_2–Y_2O_3 system, we utilized a known technique; pastes from ZrO_2 and ZrO_2–Y_2O_3 nanopowders were prepared in organic solvent [6]. The photoelectodes were formed by depositing the pastes on the glass substrates with a conductive FTO coating. The ZrO_2 and ZrO_2–Y_2O_3 layers with a thickness of about 200 nm were deposited using spin-coating method, followed by sintering at 500 °C for 30 min.

The PSC fabrication process was provided under ambient conditions with high humidity ($\sim$ 50 – 60 %) using a one-step method described previously [15]. During the fabrication process, ZrO_2-based photoelectodes were first coated with a photosensitive perovskite ($CH_3NH_3PbI_3$) layer, obtained from lead iodide and methylammonium iodide precursor solutions, followed by depositing a layer of spiro-MeO-TAD as a hole-transporting material [7,14]. The PSC fabrication process was completed by thermal evaporation of conductive Au contacts with a thickness of 50 nm using vacuum system VUP-4. As a result, we have prepared PSCs with a device architecture of glass/FTO/ZrO_2–Y_2O_3/$CH_3NH_3PbI_3$/spiro-MeOTAD/Au, in which the doping content of Y_2O_3 was varied from 0 % (undoped system) to 3 and 10 mol.%.

2.2. Characterization studies

The structure and composition of nanostructured ZrO_2–Y_2O_3 system were determined by X-ray diffraction (XRD) analysis in the 13 – 65 ° range (Cu Kα radiation) using Rigaku Corporation SmartLab 3 diffractometer. The optical properties were investigated using UV-vis double-beam spectrophotometer Shimadzu 3600 with an integrating sphere ISR-3100 (Shimadzu, Japan), followed by an analysis of diffuse reflection spectra over a wavelength range 200 – 900 nm. The morphology of the films was investigated using dual-beam scanning electron microscope (SEM) Helios NanoLab 660 (FEI, USA).

The measurements of the photovoltaic parameters for PSCs were provided under standard illumination conditions (AM1.5G) with $P_{IN} = 1000$ W/m^2 by recording the current-voltage characteristics (J–V) using Abet Technologies Solar Simulator (Abet, USA) as a light source and Keithley 4200-SCS Parameter Analyzer (USA) for recording the current-voltage characteristics (J–V). The PCE (η) of the PSC was calculated from the J–V data using the known formula:

$$\eta = \frac{J_{SC} \cdot V_{OC} \cdot FF}{P_{IN}} \cdot 100\ \%, \tag{1}$$

where J_{SC} – short-circuit current density, V_{OC} – open-circuit voltage, FF – fill factor and P_{IN} – light intensity of solar radiation.

3. Results and discussion

In Fig. 1, we present comparative data of XRD patterns for the powders of undoped ZrO_2 nanoparticles and for ZrO_2–Y_2O_3 system with Y_2O_3 doping level of 3 and 10 mol.%. XRD results for the samples, obtained using hydrothermal processing of co-precipitated zirconium and yttrium, reveal the co-existence of tetragonal ($\sim$ 53 %) and monoclinic ($\sim$ 47 %) phases in ZrO_2 nanoparticles. The addition of 3 mol.% Y_2O_3 to ZrO_2 leads to the formation of a predominantly pseudo-cubic modification of ZrO_2 (*c*-ZrO_2) and a trace amount of the monoclinic modification of *m*-ZrO_2 (up to 5 %), the addition of 10 mol.% Y_2O_3 leads to the complete disappearance of *m*-ZrO_2. The crystallite size of zirconia phases, determined by the X-ray line broadening method using the Scherrer equation, was found to be 16 and 14 nm for *m*-ZrO_2 and *t*-ZrO_2, respectively. The obtained results shows that 3 mol.% Y_2O_3 additive does not affect the crystallite size. The addition of 10 mol.% Y_2O_3 decreases the crystallite size down to 5 nm, which can be explained by the formation of the "core-shell" structure in which the shell is enriched with yttria [16].

Figure 2 shows the dependence of the diffuse reflection spectra for the powders of undoped ZrO_2 and ZrO_2–Y_2O_3 system with Y_2O_3 content of 3 and 10 mol.%. XRD data have shown that yttria doping stabilizes the high-temperature tetragonal ZrO_2 phase. This result revealed that ZrO_2–Y_2O_3 samples have a monophase structure and, thus, the semiconductor properties of these materials could be characterized by a direct transition from the

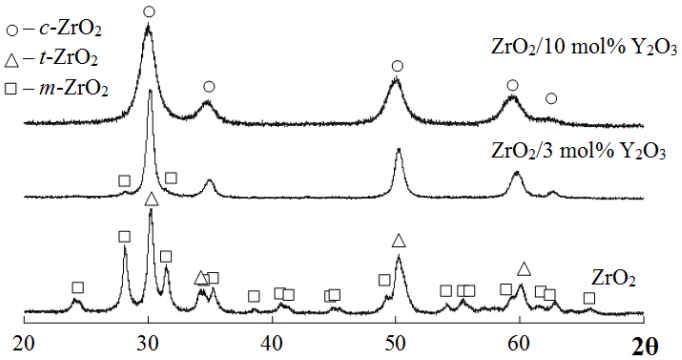

FIG. 1. XRD patterns for ZrO_2 nanoparticles with a varied Y_2O_3 content

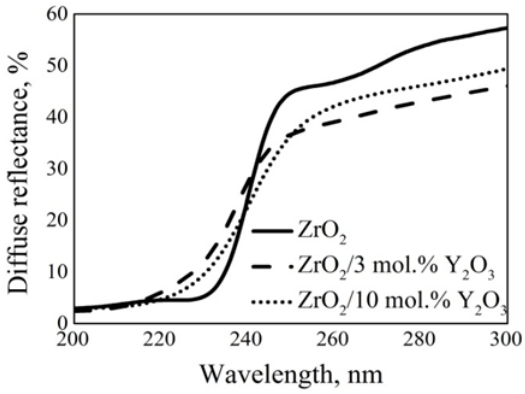

FIG. 2. Diffuse reflectance spectra for the powders of undoped ZrO_2 and ZrO_2–Y_2O_3 system

valence to the conduction band. Following the Kubelka–Munk theory, the value of the optical energy bandgap (E_g) for direct transitions can be determined from the Tauc plots [17]:

$$\alpha(h\nu) = C\frac{(h\nu - E_g)^{1/2}}{h\nu}, \tag{2}$$

where a – optical absorption coefficient, C – constant, $h\nu$ – photon energy.

The E_g values for ZrO_2 and ZrO_2–Y_2O_3 system were defined with linear extrapolation of $(\alpha h\nu)^2$ plots with the photon energy axis (Fig. 3). The results obtained showed that E_g value also enhances with the increase of doping concentration from 5.74 eV in ZrO_2 to 5.63 eV in ZrO_2–Y_2O_3 (3 %). However, in ZrO_2–Y_2O_3 (10 %), the E_g value was found to be 5.45 eV, which can be explained by a significant decrease of the nanoparticle size for that particular sample, to about 5 nm.

Typical scanning electron microscopy (SEM) surface image of the undoped ZrO_2 nanostructured layer deposited on a conductive glass substrate (Fig. 4) indicates the agglomeration of ZrO_2 sphere-like crystallites. SEM results show that the average particle size was approximately 30 – 40 nm. Fig. 5 presents the cross-sectional SEM image of the undoped ZrO_2 electron transport layer spin-coated on FTO glass substrate. It is seen that FTO conductive layer is covered with $\sim$ 200 nm uniform ZrO_2-based mesoscopic layer. Fig. 6 presents J–V characteristics, recorded for PSCs under standard illumination AM 1.5G. Photovoltaic parameters for all the investigated PSCs are summarized in Table 1. Comparative studies of the PSCs based on undoped and Y_2O_3-doped ZrO_2 photoelectrodes showed that doping leads to the increase of the short-circuit current values and improves the fill factor of the devices, resulting in the increase of total PCE values. The best performance of 11.4 % was obtained for the PSC with ZrO_2–Y_2O_3 (10 %) photoelectrode that significantly exceeds the corresponding value of 5.9 % for PSC based on undoped ZrO2 photoelectrode.

The performance of ZrO_2-based PSCs developed in this study was higher than that in TiO_2 based PSCs with much higher observed V_{OC}. The major difference between the above mentioned configurations of PSCs concerns the different charge transport mechanisms at the perovskite/photoelectrode interface for ZrO_2 and TiO_2 electrodes. Fig. 7 presents schematic energy band diagrams demonstrating the energy band structure for PSCs

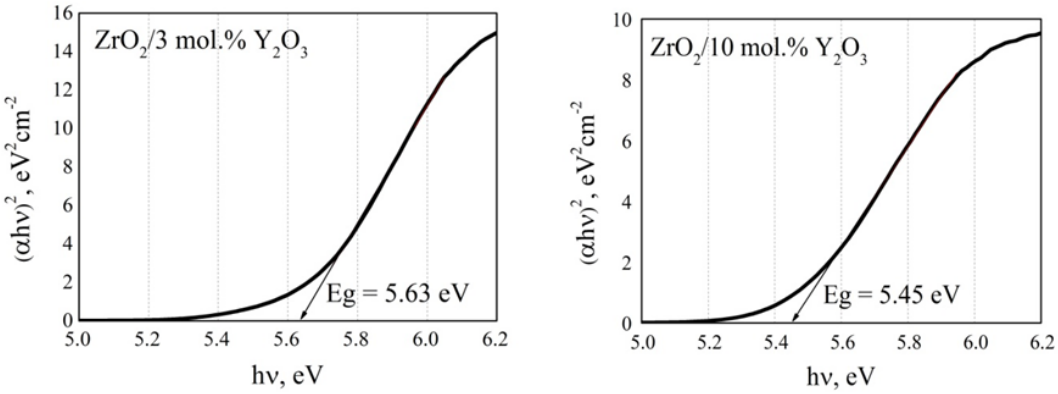

FIG. 3. E_g values for ZrO_2–Y_2O_3 system extracted from $(\alpha h\nu)^2$ vs. photon energy graphics

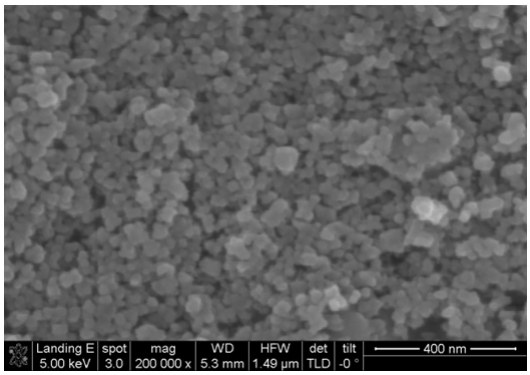

FIG. 4. SEM image of undoped ZrO_2 nanostructured layer spin-coated on a conductive glass substrate

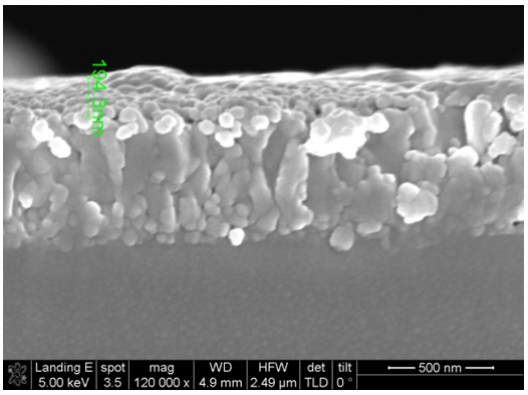

FIG. 5. Cross-sectional SEM image of the ZrO_2-based photoelectrode

TABLE 1. Photovoltaic characteristics of ZrO_2–Y_2O_3 based PSCs

PCE parameters	Photoelectrode		
	ZrO_2	ZrO_2/3 mol.% Y_2O_3	ZrO_2/10 mol.% Y_2O_3
V_{OC}, V	0.94	1.0	1.0
J_{SC}, m/m^2	10.9	13.6	15.4
FF, a.u.	0.58	0.69	0.74
η, %	5.9	9.4	11.4

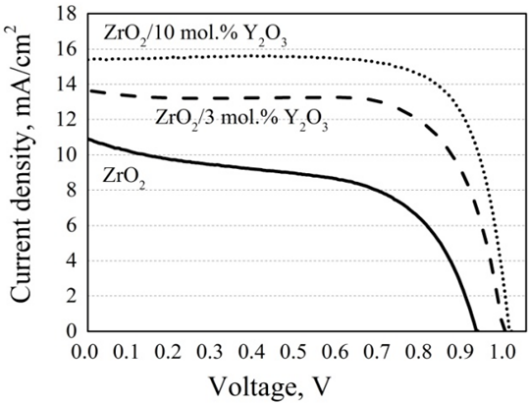

FIG. 6. J–V characteristics of the PSCs based on ZrO_2–Y_2O_3 photoelectrodes under simulated AM 1.5G (1000 W/m^2) irradiance

based on a ZrO_2 photoelectrode (Fig. 7(a)) and on traditional TiO_2 photoelectrode (Fig. 7(b)). The band diagram in Fig. 7(b) demonstrates that the conduction band edge of perovskite has the energy above the conduction band edge of TiO_2 [18] that enables a classic photoexcited electron transfer from the perovskite layer to the TiO_2 photoelectrode. Unlike the previously described situation, the conduction band edge of ZrO_2 has much higher energy (Fig. 7(a)), leaving the conduction band edge of perovskite far below, which makes it impossible to transfer the electrons from the perovskite to ZrO_2 in terms of the classical charge transfer mechanism. It is also known that under ambient temperature, ZrO_2 is an insulator with poor carrier transport characteristics and its practical applicability as a charge carrier transporting material is questionable. However, several publications confirmed that the mechanism of charge transport in nanostructured wide-bandgap electrodes, being of primary physical and technical significance, is different from that in the bulk materials [19]. It was also shown that rare earth oxide doping initiates the creation of core-shell structures and results in a high concentration of surface defects [16] that significantly improves the transport characteristics of the mesoscopic photoelectrodes and increases the efficiency of the solar cells [20, 21]. The latter is possible due the large concentration of the nanoparticle surface defects. A number of publications confirmed that in nanostructured systems with $E_g > 5$ eV, the effective transfer of the injected electrons was observed, while the density of the electrons in the conduction band was negligible [19]. In our study, we observed the effective electron conduction through the nanostructured ZrO_2 layer that can be explained on the basis of the hopping conduction mechanism through localized states within forbidden zone of ZrO_2 [10].

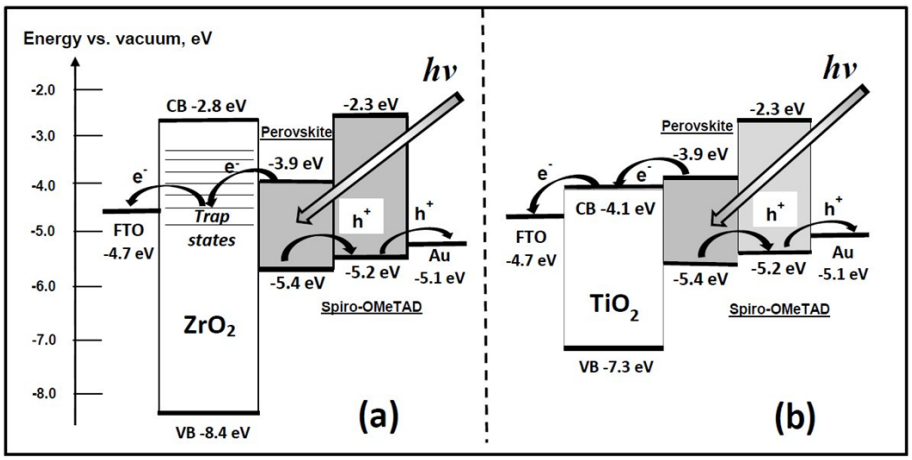

FIG. 7. Schematic energy band diagrams comparing the energy band structures for PSCs based on ZrO_2 (a) and TiO_2 photoelectrodes (b)

4. Conclusions

As a result, we have developed the technology and provided synthesis of both undoped and Y_2O_3-doped ZrO_2 nanoparticles for which the structural, optical and energy characteristics were investigated. It was found that the band-gap value in ZrO_2 decreases with increased Y_2O_3 doping. The developed materials were used for fabrication of nanostructured thin film photoelectrodes for constructing and providing a comparative study of the PSCs with the architecture of glass/FTO/ZrO_2–Y_2O_3/$CH_3NH_3PbI_3$/spiro-MeOTAD/Au. The power conversion efficiency in the PSCs based on ZrO_2–Y_2O_3 photoelectrodes was shown to be significantly higher than that for undoped ZrO_2 photoelectrodes. We have found that nanostructured layer, based on very wide-bandgap ZrO_2 nanoparticles, could efficiently transfer the injected electrons to the back contact through the hopping transport mechanism via trap states in the forbidden zone of ZrO_2. The obtained results demonstrate the possibility of using a very wide-bandgap oxide nanostructured materials with E_g values exceeding 5 eV for fabrication electron-conductive layers, including their successful application as mesoscopic photoelectrodes for perovskite solar cells.

Acknowledgements

This work was supported by the Russian Science Foundation under grant No. 17-19-01776.

References

[1] Shevaleevskiy O. The future of solar phtovoltics: from physics to chemistry. *Pure Appl. Chem.*, 2008, **80**, P. 2079–2089.
[2] Kuznetsov S.V., Morozov O.A., et al. $Ca_{1-x-y}Yb_xPr_yF_{2+x+y}$ solid solution powders as a promising materials for crystalline silicon solar energetics. *Nanosystems: Phys. Chem. Math.*, 2018, **9** (2), P. 259–262.
[3] Shi Z., Jayatissa A.H. Perovskite solar cells: from the atomic level to film quality and device performance. *Materials*, 2018, **57** (10), P. 2554–2569.
[4] Ho-Baillie A. Perovskites cover silicon textures. *Nat. Energy*, 2018, **17**, P. 751–752.
[5] Marinova N., Tress W., et al. Light harvesting and charge recombination in $CH_3NH_3PbI_3$ perovskite solar cells studied by hole transport layer thickness variation. *ACS Nano*, 2015, **9**, P. 4200–4209.
[6] Vildanova M.F., Kozlov S.S., et al. Niobium-doped titanium dioxide nanoparticles for electron transport layers in perovskite solar cells. *Nanosystems: Phys. Chem. Math.*, 2017, **8** (4), P. 540–545.
[7] Vildanova M.F., Nikolskaia A.B., et al. Novel types of dye-sensitized and perovskite-based ntandem solar cells with a common counter electrode. *Tech. Phys. Lett.*, 2018, **44** (2), P. 126–129.
[8] Kozlov D.A., Lebedev V.A., et al. The microstructure effect on the Au/TiO_2 and Ag/TiO_2 nanocomposites photocatalytic activity. *Nanosystems: Phys. Chem. Math.*, 2018, **9** (2), P. 266–278.
[9] Ganguly A., Nath S.S., Gope G., Choudhury M. CdS quantum dot sensitized zinc oxide based solar cell with aluminum counter electrode. *Nanosystems: Phys. Chem. Math.*, 2017, **8** (6), P. 782–786.
[10] Rath M.S., Ramakrishna G., Mukherjee T., Ghosh H.N. Electron injection into the surface states of ZrO_2 nanoparticles from photoexcited quinizarin and its derivatives: effect of surface modification. *J. Phys. Chem. B*, 2005, **109**, P. 20485–20492.
[11] Bugrov A.N., Almjasheva O.V. Effect of hydrothermal synthesis conditions on the morphology of ZrO_2 nanoparticles. *Nanosystems: Phys. Chem. Math.*, 2013, **4**, P. 810–815.
[12] Almjasheva O.V., Krasilin A.A., Gusarov V.V. Formation mechanism of core-shell nanocrystals obtained via dehydration of coprecipitated hydroxides at hydrothermal conditions. *Nanosystems: Phys. Chem. Math.*, 2018, **9** (4), P. 568–572.
[13] Kolesnik I.V., Lebedev. V.A., Garshev A.V. Optical Properties and photocatalytic activity of nanocrystalline TiO_2 doped by 3d-metal ions. *Nanosystems: Phys. Chem. Math.*, 2018, **9** (3), P. 401–409.
[14] Bi D., Moon S.J., et al. Using a two-step deposition technique to prepare perovskite ($ch_3nh_3pbi_3$) for thin film solar cells based on ZrO_2 and TiO_2 mesostructures. *RSC Advances*, 2013, **3** (41), P. 18762–18766.
[15] Shevaleevskiy O.I., Nikolskaia A.B., et al. Nanostructured TiO_2 Films with a Mixed Phase for Perovskite Solar Cells. *Russ. J. Phys. Chem.*, 2018, **12** (4), P. 663–669.
[16] Almjasheva O.V., Smirnov A.V., et al. Structural features of ZrO_2–Y_2O_3 and ZrO_2–Gd_2O_3 nanoparticles formed under hydrothermal conditions. *Russ. J. Gen. Chem.*, 2014, **84** (5), P. 804–809.
[17] Tauc J., Grigorovici R.,Vancu A. Optical properties and electronic structure of amorphous germanium. *Phys. St. Sol.*, 1966, **15**, P. 627–637.
[18] Kim H.-S., Lee C.-R., et al. Lead iodide perovskites all-solid-state submicron thin film mesoscopic solar cell with efficiency exceeding 9%. *Sci. Rep.*, 2012, **2**, 591.
[19] Oum K., Lohse P.W., et al. Photoinduced ultrafast dynamics of the triphenylamine-based organic sensitizer D35 on TiO_2, ZrO_2 and in acetonitrile. *Phys. Chem. Chem. Phys.*, 2013, **15**, P. 3906–3916.
[20] Nikolay T., Larina, L., Shevaleevskiy O., Ahn B.T., Electronic structure study of lightly Nb-doped TiO_2 electrode for dye-sensitized solar cells. *Energ. Environ. Sci.*, 2011, **4**, P. 1480–1486.
[21] Kozlov S., Nikolskaia A., et al. Rare-earth and Nb doping of TiO_2 nanocrystalline mesoscopic layers for high-efficiency dye-sensitized solar cells. *Phys. St. Sol. A*, 2016, **213**, P. 1801–1806.